Hindawi Publishing Corporation
Advances in Materials Science and Engineering
Volume 2012, Article ID 452383, 11 pages
doi:10.1155/2012/452383

Research Article

Electrical Properties of a CeO_2-Bi_2O_3 Mix System Elaborated at 600°C

Lamia Bourja,[1,2] Bahcine Bakiz,[1,2] Abdeljalil Benlhachemi,[2] Mohamed Ezahri,[2] Sylvie Villain,[1] Claude Favotto,[1] and Jean-Raymond Gavarri[1]

[1] *Institut Matériaux Microélectronique et Nanosciences de Provence, IM2NP, UMR CNRS 7334, Université du Sud Toulon-Var, BP 20132, 83957 La Garde Cedex, France*
[2] *Laboratoire Matériaux et Environnement LME, Faculté des Sciences, Université Ibn Zohr, BP 8106, Cité Dakhla, Agadir, Morocco*

Correspondence should be addressed to Jean-Raymond Gavarri, gavarri.jr@univ-tln.fr

Received 29 July 2011; Accepted 26 December 2011

Academic Editor: V. P. S. Awana

The electrical conduction of a series of polycristalline $[(1-x)CeO_2 \cdot x/2Bi_2O_3]$ samples has been analyzed using electrical impedance spectroscopy, in the temperature range 25 to 750°C. Samples have been prepared via a coprecipitation route followed by a pyrolysis process at 600°C. For compositions $x \leq 0.20$, $Ce_{1-x}Bi_xO_{2-x/2}$ solid solutions, with fluorite cubic structure, are obtained. In the composition range $0.30 \leq x \leq 1$, the system is biphasic with coexistence of cubic and tetragonal structures. To interpret the Nyquist representations of electrical analyses, various impedance models including constant phase elements and Warburg impedances have been used. In the biphasic range ($0.30 \leq x \leq 0.7$), the conductivity variation might be related to the increasing fraction of two tetragonal β' and β-Bi_2O_3 phases. The stabilization of the tetragonal phase coexisting with substituted ceria close to composition $x = 0.7$ is associated with a high conduction of the mix system CeO_2-Bi_2O_3.

1. Introduction

Recently, in a structural analysis [1] of the polycrystalline system $(1 - x) \cdot CeO_2 - (x/2) \cdot Bi_2O_3$ with $0 \leq x \leq 1$, elaborated at 600°C, we have observed the partial stabilization of two tetragonal varieties of Bi_2O_3 oxide coexisting with a substituted ceria phase. Presently, we analyze the electrical properties of this CeO_2-Bi_2O_3 system as a function of composition x and at various temperatures.

Cerium dioxide (ceria) is well known for its applications as ceramic pigments, solid electrolyte in fuel cells, and catalyst in automotive gas converters [2–9]. Ceria presents mixed ionic and electronic conductivity [10, 11]. In a previous work on the neodymium-substituted phase $Ce_{(1-x)}Nd_xO_{2-x/2}$ [12], we showed that the conductivity increased with composition x up to a value of $x = 0.20$ in the cubic lattice. Other studies have shown a similar effect with other elements: europium [13], iron [14], gadolinium [15], samarium [16], and terbium [17].

In 1937, Sillen [18] published the first study on the complex polymorphs of Bi_2O_3 using X-ray diffraction (XRD) analysis. Four polymorph phases were proposed: (i) the α-Bi_2O_3 monoclinic phase, stable at low temperatures; (ii) the δ-Bi_2O_3 face-centered cubic phase, stable at high temperatures (above 729°C); (iii) the two intermediate β- and γ-Bi_2O_3 phases that can stabilize with tetragonal and body-centered cubic (bcc) lattices, respectively, depending on the cooling mode. An additional polymorph was also observed by the authors [19]: a β'-Bi_2O_3 tetragonal modification that should be a superstructure of the β phase. During cooling of the high-temperature cubic δ-Bi_2O_3 phase to T = 650°C, this δ phase can transform into the β-Bi_2O_3 tetragonal modification. However, below T = 640°C, this δ phase can transform into the γ (body centered cubic) modification. If this γ phase is formed, it transforms into the α-Bi_2O_3 monoclinic phase close to 500°C. However, if the β phase is formed, it transforms into the α phase close to 330°C [20–22].

Several studies on the electrical properties of Bi_2O_3 [22–28] have shown that conduction is mainly ionic above 500°C. According to the authors, this ionic conduction should be favored by the existence of vacancies or empty spaces in the high-temperature structure that allows fast mobility of the oxygen ions in the lattice. Chemical units noted as $Bi_4O_6\square_2$ are organized into a structure that is closely related to that of fluorite (basic A_4O_8 units). Both cerium and bismuth oxides should exhibit similar crystal packing in which the oxygen vacancies are associated with the Bi^{3+} ions: the ceria chemical unit Ce_4O_8 might be converted into the $Bi_4O_6\square_2$ chemical unit in which the Bi^{3+} ions substitute for the Ce^{4+} ions and oxygen vacancies substitute for the oxygen atoms. Some authors have proposed that the presence of lone pairs could play a role in the observed phase transition α (monoclinic) $\rightarrow$ δ (cubic) at 729°C and in the measured high conductivity.

The substituted phases $Ce_{1-x}Bi_xO_{2-\delta}$ have already been studied by Dikmen et al. [29], and the solubility limit was found to be $x < 0.25$. However, very few data are available on the section of the phase diagram with $x > 0.25$.

It is interesting to note that the authors Chen and Eysel [30] studied the composite system CeO_2-Bi_2O_3 in the composition range $x = 0.7$ to $x = 1$ and observed that the metastable β phase was stabilized by the presence of the ceria phase. They suggest that this stabilization should be provoked by a certain proximity effect. They considered that this stabilization was not due to any insertion of cerium ions in the Bi_2O_3 lattice.

Recently, using hydrothermal route, Sardar et al. [31] synthesized $Ce^{4+}{}_{1-x}Bi^{3+}{}_xO_{2-\delta}$ phases with $x < 0.6$ having ceria-like fluorite structure with local distortions.

In our previous work [1], we observed at least three domains for these samples obtained at 600°C. In agreement with literature results, a first solid-solution domain was observed for $x < 0.30$, with a limiting composition close to $x = 0.20$. Surprisingly, we also found evidence for a second biphasic system with $0.30 \leq x \leq 0.70$, which should be constituted of the limit phase with $x = 0.20$ coexisting with a tetragonal phase quite similar to the β'-Bi_2O_3 phase. A third biphasic system was also observed for $0.80 \leq x \leq 0.90$, with coexistence of the tetragonal β-Bi_2O_3 phase and the monoclinic α-Bi_2O_3 phase, which is stable at low temperatures. The tetragonal β' polymorph (lattice parameters: $a = 0.15542$ nm; $c = 0.5645$ nm) is a superstructure of the β phase (lattice parameters: $a = 0.7742$ nm; $c = 0.5633$ nm). In the past, both phases were considered to be metastable varieties of pure Bi_2O_3 oxide. In our specific case, the modification $\beta' \leftrightarrow \beta$ depending on composition x should result from ordering-disordering of cerium defects in the lattice: ordering (β' phase stabilization) should require sufficient fraction of cerium atoms in the lattice, while disordering (β phase stabilization) should be due to insufficient fraction of cerium atoms in the lattice. Finally, for $x = 1$, we obtained a stable monoclinic structure (lattice parameters: $a = 0.5853$ nm; $b = 0.8169$ nm; $c = 0.7516$ nm; $\beta = 112.95°$). In our study, we also observed typical variations in the volumes of the chemical units A_4O_8 (Ce_4O_8 for the ceria structure and $Bi_4O_6\square_2$ for the β' and β phases). For compositions $x < 0.30$, the volume increase is directly due to the increased Bi^{3+} fraction. For compositions $0.3 \leq x \leq 0.7$, the volume increase can be interpreted in terms of the increasing fraction of metastable phase β'-Bi_2O_3 coupled with a decreasing fraction of defects in the Bi_2O_3 lattice. For compositions $0.7 \leq x \leq 0.9$, the volume reaches a stabilized value due to the very weak concentration of cerium defects. The large decrease in volume for $x = 1$ should be due to the formation of the more compact monoclinic α-Bi_2O_3 structure. These variations are reported on Figure 1 (see [1]).

At present, we are trying to elucidate the role of the bismuth composition on the ionic conduction of this mixed system. Such composite systems could present a very high interest in the case of electrolytic applications.

2. Experimental Section

2.1. Sample Elaboration. Samples of bismuth/cerium-based precursors having the composition $(1-x)CeO_2 \cdot (x/2)Bi_2O_3$ with $0 \leq x \leq 1$ were prepared via a precipitation route [32–36] using appropriate quantities of cerium(III) nitrate hexahydrate, $Ce(NO_3)_3 \cdot 6H_2O$ (purity 99.5%), and bismuth(III) nitrate pentahydrate $Bi(NO_3)_3 \cdot 5H_2O$ (purity $\geq$ 98%). Each nitrate was separately dissolved in suitable volumes of distilled water. The two nitrate solutions were mixed and stirred for two hours at room temperature. Ammonium hydroxide (NH_4OH) was added to the mixture to adjust the pH to 10. The resulting precipitate was filtered, washed with distilled water to remove residual $NH_4{}^+$, and dried at 80°C. Finally, the precursor powder was heated in air at 600°C for 6 hours. We obtained eleven samples of compositions $x = 0$, 0.10, 0.20, 0.30, 0.40, 0.50, 0.60, 0.70, 0.80, 0.90, and 1.00. In Table 1, we report the experimental and calculated densities, the apparent porosities ($P = 1 - \mu_{exp}/\mu_{calc}$), and grain sizes [1]. The μ_{calc} calculated density is obtained from a theoretical evaluation taking into account a mean molar mass (A_4O_8 formula depending on composition x) and a mean volume of chemical unit A_4O_8 (see Figure 1) depending on composition x, determined from the crystal structure of each phase. In the mix system where substituted ceria and tetragonal phases (β' or β) coexist, the phase ratio has been calculated using the classical lever rule.

2.2. Electrical Analyses. The electrical study was performed using an electrical impedance spectrometer SOLARTRON SI 1260 coupled to an electrical cell operating under air and in the temperature range from 25 to 750°C. The samples were cylindrical pellets (diameter 12.8 $\pm$ 0.1 mm, thickness 2 $\pm$ 0.05 mm) initially compacted at 5 kbar under ambient conditions. Each apparent density was calculated and compared with the theoretical value to determine the fraction of cavities. The pellets were placed between two cylindrical platinum electrodes in a specific cell. A constant pressure was applied to the electrodes via rings. The cell was placed in a furnace operating at up to 750°C.

The electrical analyses were carried out in the frequency range ($\omega = 2\pi\nu$) 10^{-1} to 10^7 Hz, with an alternating current associated with a maximum voltage of 0.1 V. Samples were

Table 1: Sample characteristics (densities, grain sizes, and porosities).

Composition x	Average crystallites size D (nm) CFC (ceria)		Experimental density μ_{exp} ($g\cdot cm^{-3}$)	Calculated density μ_{calc} ($g\cdot cm^{-3}$)	Porosity P
0	22		6.65	7.20	0.08
0.1	20		6.93	7.44	0.07
0.2	19		7.12	7.68	0.07
		β' (Bi_2O_3)			
0.3	11	20	7.71	8.50	0.09
0.4	10	29	7.94	8.52	0.07
0.5	10	34	7.98	8.52	0.06
0.6	10	36	8.02	8.53	0.06
0.7	10	38	7.94	8.53	0.07
		β (Bi_2O_3)			
0.8		78	8.06	8.68	0.07
0.9		85	8.14	8.93	0.09
		α (Bi_2O_3)			
1		181	8.73	9.36	0.07

Note: μ_{exp} ($g\cdot cm^{-3}$) = m/V; $P = 1 - \mu_{exp}/\mu_{calc}$.

stabilized for 15 minutes at a fixed temperature. The recording time for the frequency range was of 15 minutes. To ensure thermal stabilization of pellets, each sample was subjected to three successive measuring cycles (with one temperature rise and drop for each cycle). The final impedance data were chosen during heating mode of the third cycles, as being representative of stabilized samples (these data were identical to those of the second cycle).

The impedances $Z = Z' + jZ''$ (Z' and Z'' being, resp., the real and imaginary components) were represented using Nyquist plots ($X = Z'$, $Y = -Z''$). The software Zview [37] was used to fit the impedances of specific electrical circuits to the Nyquist experimental data (Nyquist representations). The equivalent circuits associated with each sample were generally based on parallel RC circuits; constant-phase elements Z(CPE) having the form $1/Z(\text{CPE}) = A\cdot(j\omega)^n$ were systematically tested. At low temperature ($\Theta < 500°C$), the impedance of such parallel RC circuits is generally expressed as a function of frequency ω as follows:

$$\frac{1}{Z} = \frac{1}{R} + A(j\omega)^n \quad \text{or} \quad Z = \frac{R}{\left[1 + R\cdot A\cdot (j\omega)^n\right]}. \tag{1}$$

In these expressions, R is the resistance (associated with the intersection of the Nyquist circle with real Z' axis), the CPE term A is expressed in $\Omega^{-1}\cdot Hz^{-n}$, the frequency ω is expressed in Hz, n is the exponent describing the deviation from the ideal capacitor model and is characteristic of the CPE model.

In the case of high temperature results ($\Theta > 500°C$), it has been necessary to use a specific modified Warburg model [38–42] having the following form:

$$Z_w = R_w\cdot \text{Tanh}\frac{\left[(jA_w\omega)^n\right]}{(jA_w\omega)^n}, \tag{2}$$

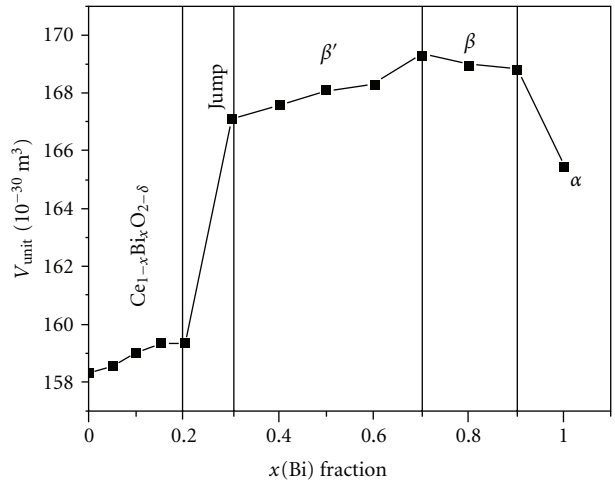

Figure 1: Variation of the A_4O_8 unit volume V_{unit} versus bismuth fraction x (from [1]). (1): for $0 \le x \le 0.2$, Ce_4O_8 unit for the solid solution $Ce_{(1-x)}Bi_xO_{(2-\delta)}$. (2): for $0.3 \le x \le 0.7$, $Bi_4O_6\square_2$ unit for the tetragonal β' phase. (3) for $0.7 < x < 0.9$, $Bi_4O_6\square_2$ unit for the tetragonal β phase. (4) for $x = 0.7$ maximum of conduction due to the tetragonal phase. (5) for $x = 1$, $Bi_4O_6\square_2$ unit for the monoclinic α phase.

with R_w as a specific resistance (in Ω), A_w as a specific term depending on diffusion mechanisms, related to the electrode or interface responses (see the appendix), and n being an exponent characteristic of the diffusion process coupled with the sample heterogeneity. In the case of pure Warburg diffusion mechanism, this n value should be equal to 1/2.

Three circuits placed in series were systematically tested for grain core, grain interface, and electrode contributions. At high temperature, the high frequency impedances for compositions $x > 0.3$ included an inductance L term. The

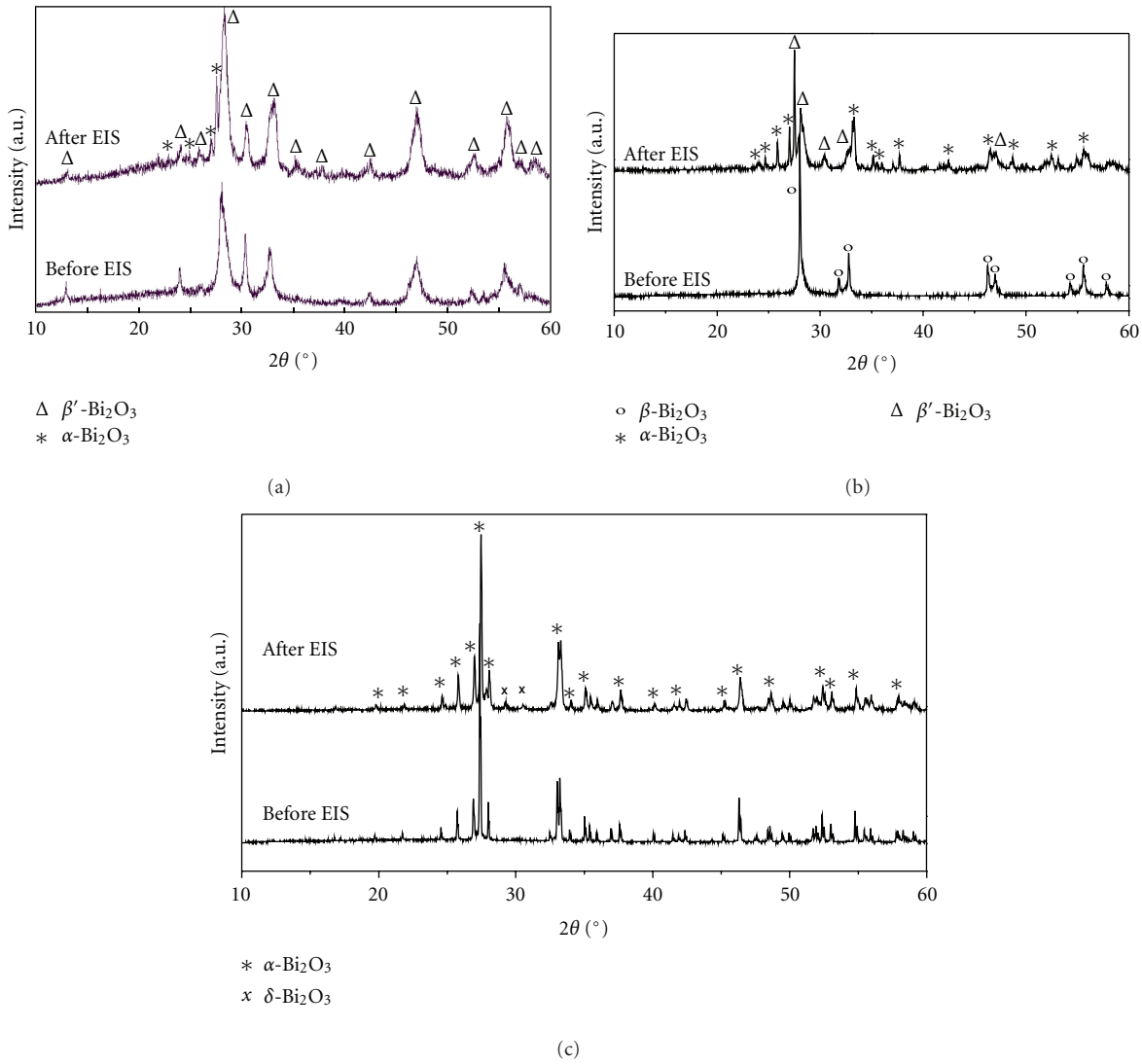

FIGURE 2: XRD patterns ($\lambda_{\text{cuK}\alpha 1} = 1.54 \times 10^{-10}$ m) before and after EIS experiments. (a) $x = 0.7$ (phase β'); (b) $x = 0.8$ (phase β); (c) $x = 1$ (phase α).

results of fitting calculations delivered the R, A, and L parameters, the Warburg characteristics (for high temperatures) of samples. All observed impedances Z_{obs} were normalized using the dimensions of each pellet (surface S and thickness L). As these dimensions were constant for all samples, no correction was necessary.

3. Results

3.1. Phase Identification after Thermal Cycles. In this section, we report a phase identification of typical samples before and after electrical analyses (each sample subjected to three thermal cycles). Let us recall that these identifications were carried out in room conditions, for samples initially elaborated at 600°C and then thermally treated up to 750°C during EIS analyses. Scanning electron microscopy images have been presented and commented in our previous work [1].

Figures 2(a), 2(b), and 2(c), respectively, report the six X-ray diffraction patterns for samples $x = 0.7$ (phase β'), $x = 0.8$ (phase β), and $x = 1$ (phase α) recorded in room conditions before and after EIS cycles. These analyses, performed before and after EIS experiments, clearly show that, after successive thermal treatments, three types of complex stabilized systems are formed and observable at 25°C. For composition $x = 0.7$, the major β' phase coexists with traces of monoclinic α-Bi_2O_3 phase; for composition $x = 0.8$, the β phase is changed into the β' phase coexisting with the monoclinic phase; for composition $x = 1$, α-Bi_2O_3 monoclinic and traces of δ-Bi_2O_3 cubic phase coexist. The presence of this cubic phase in this last sample is probably due to structural quenching during cooling process from 750°C. The presence of traces of monoclinic form in samples $x = 0.7$ and $x = 0.8$ may be interpreted in terms of diffusion of defects from the tetragonal phases.

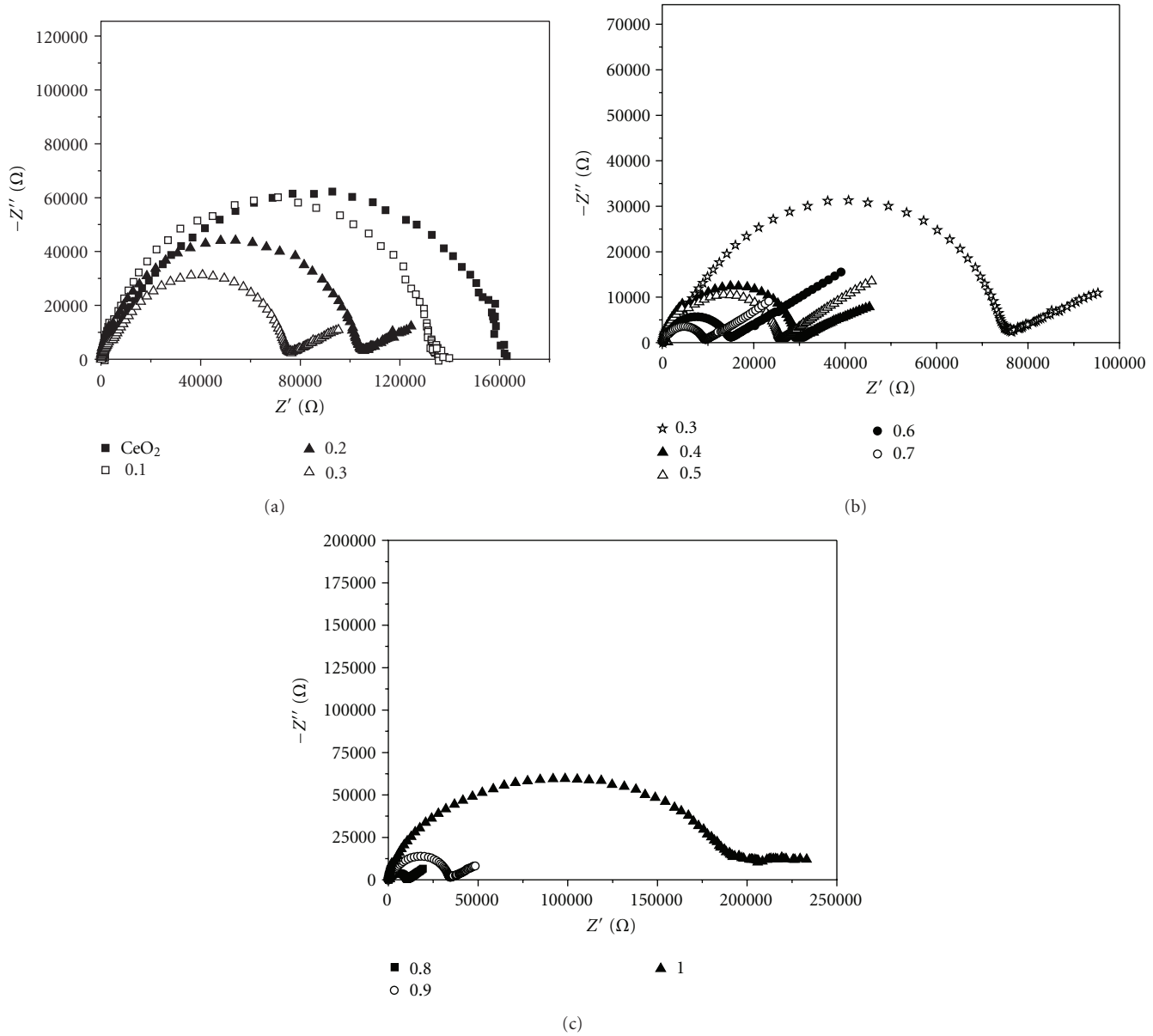

Figure 3: Nyquist plots of impedance analyses at 400°C for the system $(1 - x)CeO_2 \cdot (x/2)Bi_2O_3$. Depletion angles of Nyquist circles are visible. The low-frequency signals are associated with Warburg-like behaviors. (a) $0 < x < 0.3$; (b) $0.3 < x < 0.7$; (c) $0.7 < x < 1$.

3.2. Electrical Properties. Figure 3 represents a series of Nyquist plots at 400°C for the 11 samples. Below composition $x = 0.20$, the plots constitute unique Nyquist circles associated with grain-core conduction. Above composition $x = 0.20$, two circles are observed (associated with grain-boundary and grain-core conduction) with a linear contribution at low frequency corresponding to conduction and diffusion at the electrodes. This contribution might be assimilated mainly to an ionic conduction corresponding to ionic diffusion along grain boundaries and at the electrode interfaces.

On Figures 4(a) and 4(b), we have represented a series of Nyquist plots at 600, 650, 700, and 750°C for composition $x = 0.7$.

On Figures 5(a), 5(b), 5(c), and 5(d), we have reported a part of the results of modeling calculations, with corresponding equivalent circuits. Figure 5(a) is relative to sample $x = 0$ (ceria) with equivalent circuit $Z = Z_1$ at 700°C. Figure 5(b) is relative to sample $x = 0.2$ with model $Z = Z_1 + Z_w$ at 400°C. Figure 5(c) is relative to sample $x = 0.5$ with equivalent circuit $Z = Z_1 + Z_2 + Z_w$ at 300°C. Figure 5(d) is relative to sample $x = 0.8$ with equivalent circuit $Z = Z_3 + Z_4 + Z_w$ at 600°C.

For temperatures $\Theta < 500$°C, the impedance is given by $1/Z_1 = 1/R_1 + A_1(j \cdot \omega)^{n_1}$. The results concerning the CPE terms $A_1(j\omega)^{n_1}$ for typical temperatures (300, 350, 400, and 450°C) are reported in Table 2(a). The resistance values R_1 are not reported here (see Figure 6 representing

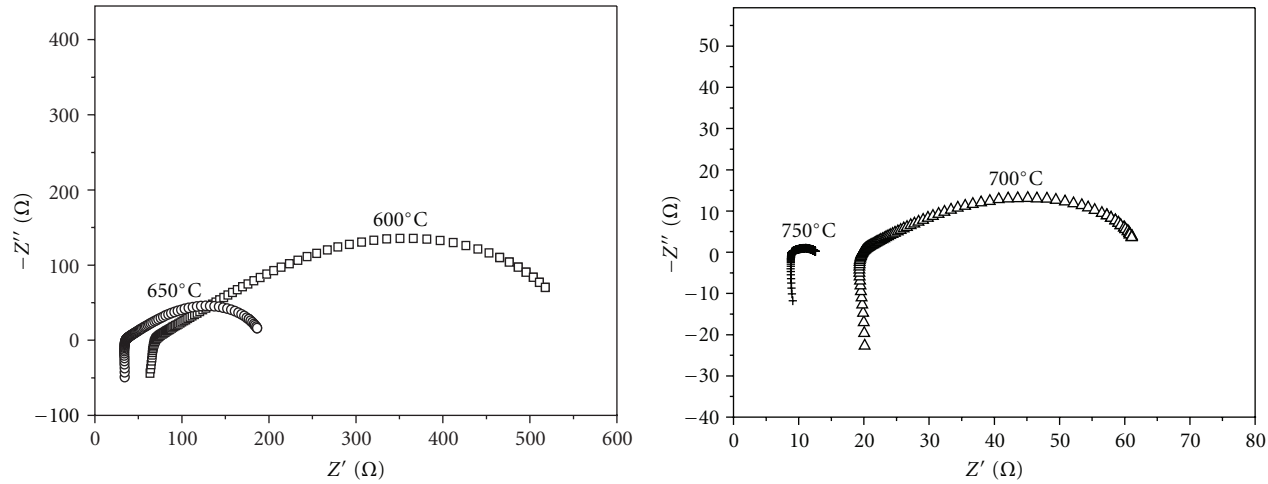

Figure 4: Nyquist representations for the $(1 - x)CeO_2 \cdot x/2Bi_2O_3$ sample with $x = 0.7$ at various temperatures. This composite sample presents an optimal conductivity.

the conductivity *versus* temperature and composition). The A_1 values increase as composition x (or temperature Θ) increases, and the n_1 values determined at low temperatures ($\Theta < 450°C$) decrease from 0.9 and 0.8 as temperature increases.

In the high temperature range ($\Theta > 500°C$), the Z values can be described from several electrical components including an inductance L_0. The general Z value has been expressed using three components as follows: $Z = Z_3 + Z_4 + Z_w$. The term $Z_3 = R_3 + jL\omega$ should represent external electrical terminals (metallic junctions) mixed with a main sample contribution (grain core): as R_3 depends on composition and temperature, it cannot be linked to such metallic contributions. The term Z_4 has a CPE form and can be linked to sample interfaces: $1/Z_4 = 1/R_4 + A_4(j\omega)^{n_4}$. The term Z_w should represent the electrode contribution. We have observed that a typical modified Warburg form could better describe the Nyquist curves (Z_w contribution). It is the reason why we did not use the usual CPE form. As the R_3, R_4, and R_w values strongly decrease with temperature, we have considered that they were mainly associated with sample and/or interface evolutions including electrode-sample interfaces. The sample resistance was determined as being the sole R_3 term representing the bulk properties.

In Table 2(b), we have reported a series of results concerning a typical sample at composition $x = 0.70$ and for various temperatures. This table is decomposed into three sections corresponding to three temperature ranges: $\Theta < 250°C$ (Z_1 component), $250 < \Theta < 500°C$ ($Z_1 + Z_2$), $500 < \Theta < 750°C$ ($Z_3 + Z_4 + Z_w$).

The A_1 values associated with grain cores (sample $x = 0.7$) increase as a function of temperature. The n_1 values decrease from $n_1 = 1$ to $n_1 = 0.8$. The thermal variations of the characteristics (A_2, n_2), and (A_w, n_w) are related to the thermal evolutions of heterogeneous grain boundaries and heterogeneous electrode-material junctions.

The n_2 values decrease (from 0.7 to 0.5) and the A_2 values increase as a function of temperature, between 300 and 450°C. The R_3, R_4, and R_w values decrease as temperature increases. The mean n_4 values are close to 0.65. The n_w values are close to 0.3. These low values of exponents validate the existence of diffusional process linked to ionic conduction. The values of A_4 increase with temperature, while the A_w term seems to irregularly vary.

In Table 2(c), we have reported partial results concerning a series of samples (variable composition $x > 0.2$) at a fixed temperature of 700°C. In the composition range $0 < x < 0.2$, the impedance model is $1/Z_1 = 1/R_1 + A_1 \cdot (j\omega)^{n_1}$. Above $x = 0.2$, the impedance model is expressed as being $Z = Z_3 + Z_4 + Z_w$.

At this high temperature, electrical evolutions are described through the following typical fitting parameters:

(i) the R_3 values (grain core) reach a minimum for compositions close to $x = 0.7$;

(ii) the R_4 values (electrode-sample interface) vary in an irregular way;

(iii) the A_4 values (electrode-sample interface) increase with x;

(iv) the n_4 values irregularly vary close to a mean value of 0.5;

(v) the R_w resistances decrease with composition x;

(vi) the A_w values (Warburg diffusion component) increase with x;

(vii) the n_w values irregularly vary close to the mean value of 0.35.

It should be remarked that the exponent n_4 is close to 0.5, while the exponent n_w is less than 0.5 (expected theoretical Warburg value).

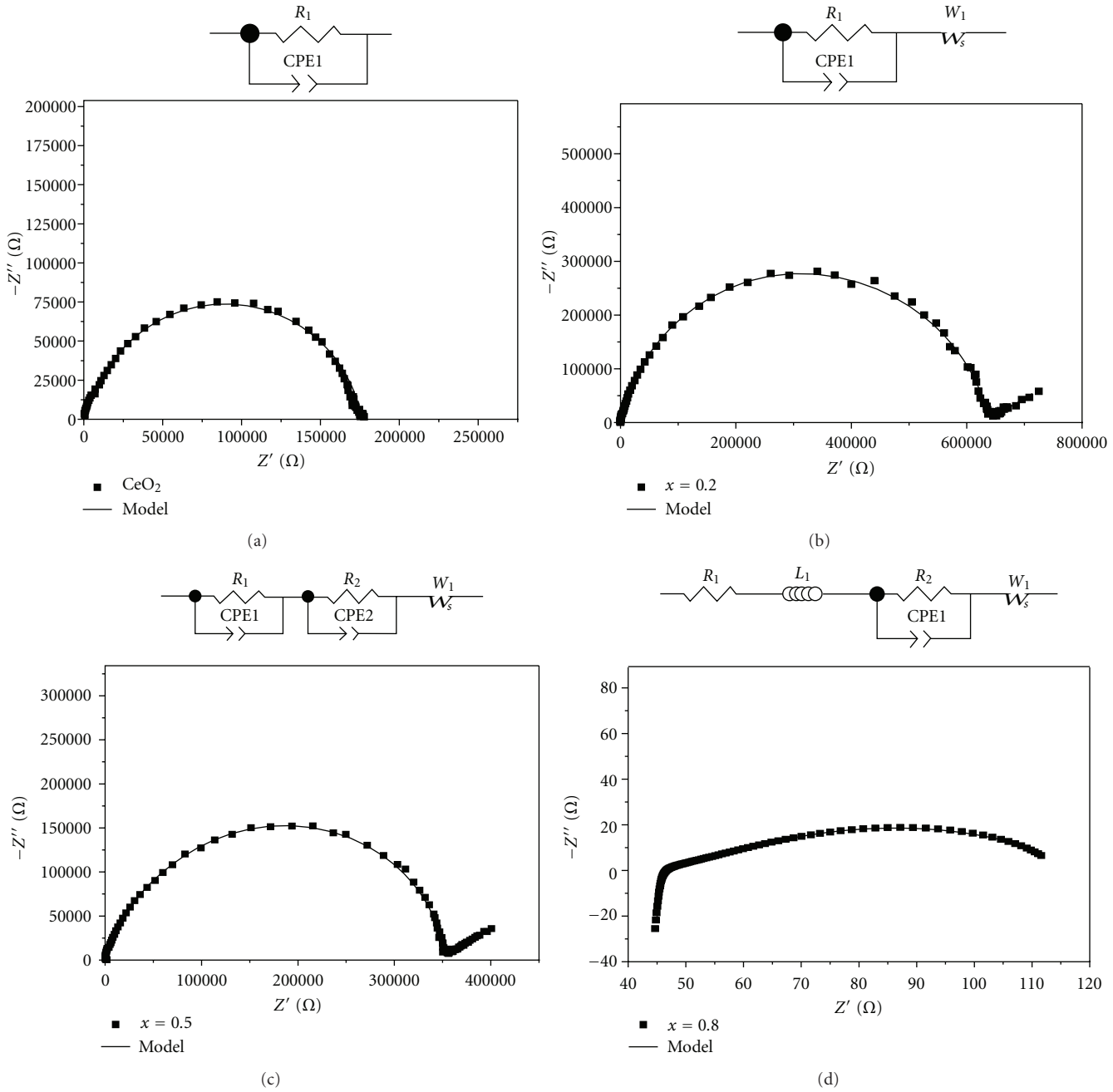

Figure 5: Comparison between calculated and experimental Nyquist representations. (a): Sample $x = 0$; (b): sample $x = 0.2$; (c): $x = 0.5$; (d): $x = 0.8$.

Figure 6 gives the values of the logarithm of conductivity $\log(\sigma)$ as a function of the composition x and for temperatures ranging between 400 and 750°C. The σ values were determined from the R_1 values and sample dimensions. Table 3 gives the values of the activation energies E_{act} as a function of composition x and for various temperature ranges. At low temperatures, low values of activation energies due to extrinsic defects are observed (close to 0.3 ± 0.1 eV). In the temperature range $400 < \Theta < 750$°C and for compositions $x < 0.4$, the activation energy first decreases from $E_a = 1.2$ to 1.09 eV then increases up to 1.19 eV. For compositions $x > 0.5$, we observe a modification in activation energy above 500°C: in the temperature range $200 < \Theta < 500$°C, this activation energy E_a is of about 1.35 eV while between 500 and 750°C, it decreases to a value of 1.0 eV. This modification might be related to a change in charge carriers with probably a significant contribution of ionic conduction.

Finally, the observed increasing conductivity as x increases should have two complementary origins: increasing

charge carriers due to Bi^{3+} and vacancies increasing fractions, and lattice energy softening due to Bi–O bonds (the activation energy being closely related to the lattice energy). This type of effect was previously suggested by Mandal et al. [43].

4. Discussion

The values of apparent conductivities, presently determined in our specific conditions, depend on experimental parameters, for example, compaction pressure, porosity, and grain sizes. These values are weaker than the values obtained by Hull et al. [28] for samples sintered at various temperatures ranging between 900 and 1300°C and corresponding to compositions $x \leq 0.3$ (solid solution). This can be easily explained first by the fact that our samples were initially sintered at 600°C then heated up to 750°C during electrical measurements and secondly by the fact that they present a certain degree of porosity (see Table 1). In the case of mix systems with high x values, it is not possible to exceed the fusion temperature of Bi_2O_3 ($\Theta = 827$°C) while this is fully acceptable in the case of solid solutions for low x values.

In the composition range $0 \leq x \leq 0.20$, the $\log(\sigma)$ values (Figure 5) increase with composition x. For these samples, the nature of conduction is probably electronic and ionic. The ionic contribution can be directly attributed to the increasing number of structural defects Bi^{3+}–□–Bi^{3+} that can offer a great number of diffusion paths for oxygen ions through the oxygen vacancies □.

In the composition range $0.30 \leq x \leq 0.70$, we have observed a new evolution with a maximum of conductivity at $x = 0.70$. This evolution might be clearly ascribed to the existence of a biphasic solid-solution system based on a solid solution having a ceria structure with disordered Bi^{3+} and vacancy defects, coexisting with a tetragonal β'-Bi_2O_3 lattice that probably has cerium defects. As the proportion of the highly conducting Bi_2O_3 phase increases, the ionic conduction also increases. For compositions greater than $x = 0.70$, the conductivity decreases. Two effects are in competition in these conductivity values: the high ionic conduction of the bismuth phase and the microstructure of the samples. As shown in our previous work [1], the specific surface areas exhibit a strong variation as x increases. In the solid-solution range $x < 0.3$, the BET analyses showed that specific surface areas are very high, whereas the specific surface areas strongly decrease as x increases in the biphasic system due to crystal growth of the bismuth phase. Thus, this evolving microstructure in the compacted pellets could play a prominent role in conduction. Cavities may play a decisive role in ionic conduction due to the formation of the tetragonal β phase.

Finally, in the case of the monoclinic Bi_2O_3 phase obtained for $x = 1$, the observed large conductivity decrease can be attributed to the more compact monoclinic structure compared to the previous tetragonal ones, which limits oxygen mobility. For this monoclinic Bi_2O_3 phase, we have observed the expected transition [20, 23, 24] at $\Theta = 740$°C, with a large increase in conductivity due to the structural transformation involving a specific volume increase (monoclinic phase transforming into the cubic phase).

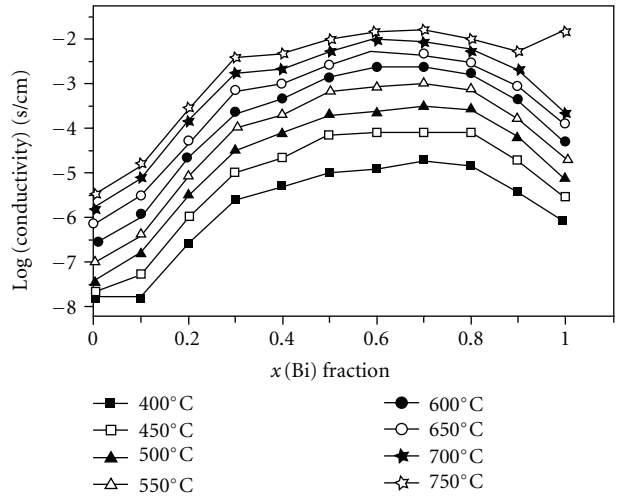

Figure 6: Evolution of sample conductivity for the system $(1 - x)CeO_2 \cdot (x/2)Bi_2O_3$ as a function of composition x and for various temperatures. The monoclinic transition is observed between 700 and 750°C in the diagram ($x = 1$) with a large $\log(\sigma)$ jump.

5. Conclusions

In this CeO_2-Bi_2O_3 system produced at 600°C under air, the main result should reside in the high conductivity of the polycrystalline and compacted mix system with compositions x close to 0.6-0.7. In this composition range, the stabilization of the β' tetragonal phase should be responsible for such a high conductivity. In our EIS experiments, this complex system is stabilized after two thermal cycles. In the composition range $0.3 \leq x \leq 0.7$, we observe a large increase in conductivity mainly due to ionic conduction of oxygen ions in this tetragonal β'-Bi_2O_3 lattice. This ionic conduction is clearly suggested by the Warburg components in Nyquist representations (for $\Theta > 300$°C). For compositions $0.7 < x < 1$, a new tetragonal structure β-Bi_2O_3 is formed at 600°C: however, it evolves after thermal treatment and gives rise to a more complex system where β' and α phases coexist. This modification of the β phase into β' and α phases might be ascribed to thermal cycling up to 750°C involving ionic diffusion: this should argue in favor of a higher stability of the β' phase due to a sufficiently proportion of cerium ions in the tetragonal lattice. For $x = 1$, the monoclinic α-Bi_2O_3 phase systematically presents a conductivity lower than the one of the mix system with composition $x = 0.7$.

Finally, the mix system with composition close to $x = 0.7$ should be an interesting optimized electrolyte for applications limited to temperatures of 700°C: below this temperature, the stability of the system should be ensured.

Table 2: (a) Electrical characteristics of compacted samples: CPE terms A_1 (in $\Omega^{-1}\cdot Hz^{-n}$ unit) and CPE exponents n, as a function of composition and for various temperatures $\Theta \leq 450°C$; 10% error for A_1 and n parameters. (b) Modeling parameters for $x = 0.7$ sample as a function of temperature Θ: resistances R_i (in Ω), CPE terms A_i (in $\Omega^{-1}\cdot Hz^{-n}$), A_w (in s) and exponents n. Three types of impedance models have been used to interpret the results. (c) Modeling parameters as a function of composition x, at 700°C: resistances R_i (in Ω), CPE terms A_i (in $\Omega^{-1}\cdot Hz^{-n}$), A_w (in s) and exponents n. Two types of impedance models have been used to interpret the results.

(a)

x	$\Theta = 300°C$		$\Theta = 350°C$		$\Theta = 400°C$		$\Theta = 450°C$	
	A_1 in $10^{-11}\,\Omega^{-1}\cdot Hz^{-n}$	n_1	A_1 in $10^{-11}\Omega^{-1}\cdot Hz^{-n}$	n_1	A_1 in $10^{-11}\,\Omega^{-1}\cdot Hz^{-n}$	n_1	A_1 in $10^{-11}\,\Omega^{-1}\cdot Hz^{-n}$	n_1
0.0	2.5	0.90	3.0	0.92	3.7	0.93	4.2	0.91
0.10	1.7	0.94	1.9	0.94	2.8	0.91	2.9	0.91
0.20	2.4	0.91	3.2	0.92	3.6	0.91	3.8	0.90
0.30	6.5	0.92	6.3	0.93	7.6	0.96	9.2	0.96
0.40	3.3	0.94	6.4	0.96	7.7	0.96	15.4	0.88
0.50	6.5	0.96	6.3	0.94	8.5	0.94	36.2	0.88
0.60	11.0	0.93	12.7	0.94	22.8	0.91	31.8	0.86
0.70	13.2	0.93	18.7	0.94	36.1	0.90	39.8	0.81
0.80	15.2	0.92	26.5	0.90	47.5	0.87	42.9	0.87
0.90	13.1	0.91	11.2	0.94	16.5	0.90	51.9	0.88
1.00	14.8	0.86	23.2	0.85	28.0	0.84	40.5	0.80

(b)

Model $1/Z_1 = 1/R_1 + A_1 \cdot (j\omega)^{n_1}$

Θ (°C)	R_1 in $10^6\,\Omega$	A_1 in $10^{-11}\,\Omega^{-1}\cdot Hz^{-n}$	n_1
110	932	9.9	0.97
150	482	8.1	0.98
200	191	10.9	0.87
250	8	33.7	0.81
% error	5%	10%	10%

Model $Z_1 + Z_2$; $1/Z_1 = 1/R_1 + A_1 \cdot (j\omega)^{n_1}$; $1/Z_2 = 1/R_2 + A_2 \cdot (j\omega)^{n_2}$

Θ (°C)	R_1 in $10^3 \cdot \Omega$	A_1 in $10^{-11}\,\Omega^{-1}\cdot Hz^{-n}$	n_1	R_2 in $10^3\,\Omega$	A_2 in $10^{-11}\,\Omega^{-1}\cdot Hz^{-n}$	n_2
300	667	13	0.93	124	30	0.78
350	58	18	0.92	12	200	0.61
400	8	36	0.90	7	2400	0.54
450	2	39	0.81	3	2000	0.51
% error	5%	10%	10%	5%	10%	10%

Model $Z = Z_3 + Z_4 + Z_w$

$Z_3 = R_3 + jL\omega$; $1/Z_4 = 1/R_4 + A_4(j\omega)^{n4}$; $Z_w = R_w \cdot \mathrm{Tanh}[(jA_w\omega)^{nw}]/(jA_w\omega)^{nw}$

Θ (°C)	R_3 (Ω)	L in 10^{-6} H	R_4 (Ω)	A_4 in $10^{-6}\,\Omega^{-1}\cdot Hz^{-n}$	n_4	R_w (Ω)	A_w in 10^{-3} s	n_w
560	109	1.4	1034	120	0.67	258.0	7.9	0.25
600	84	3.1	172	400	0.72	71.0	8.5	0.27
650	32	3.5	126	3400	0.71	43.0	3.2	0.30
700	19	2.4	22	2800	0.54	24.0	18.0	0.41
750	12	3.6	3	7700	0.59	0.3	0.1	0.37
% error	5%	10%	5%	10%	10%	10%	10%	10%

(c)

Model $1/Z_1 = 1/R_1 + A_1 \cdot (j \cdot \omega)^{n_1}$

Fraction x	R_1 in 10^4 (Ω)	A_1 in $10^{-11}\ \Omega^{-1}\cdot Hz^{-n}$	n_1
0	12	7.1	0.86
0.1	2	9.6	0.85

(c) Continued.

Model $1/Z_1 = 1/R_1 + A_1 \cdot (j \cdot \omega)^{n_1}$			
Fraction x	R_1 in 10^4 (Ω)	A_1 in 10^{-11} $\Omega^{-1}\cdot Hz^{-n}$	n_1
0.2	1	33.2	0.80
% error	5%	10%	10%

Model $Z = Z_3 + Z_4 + Z_w$

$Z_3 = R_3 + jL\omega; 1/Z_4 = 1/R_4 + A_4 \cdot (j\omega)^{n_4}; Z_w = R_w \cdot \mathrm{Tanh}[(jA_w\omega)^{nw}]/(jA_w\omega)^{nw}$

Fraction x	R_3 (Ω)	L in 10^{-6} (H)	R_4 (Ω)	A_4 in 10^{-4} $\Omega^{-1}\cdot Hz^{-n}$	n_4	R_w (Ω)	A_w in 10^{-3} s	n_w
0.3	99	2.2	10	4.3	0.54	49	1.8	0.32
0.4	76	3.2	24	2.6	0.58	45	3.2	0.40
0.5	26	3.4	6	4.4	0.73	26	6.0	0.40
0.6	16	3.6	13	10.8	0.70	27	15.0	0.40
0.7	19	2.4	22	28.0	0.54	24	18.0	0.41
0.8	24	3.6	2	43.1	0.35	20	25.0	0.35
0.9	61	2.4	4	38.3	0.45	25	12.4	0.34
% error	5%	10%	5%	10%	10%	10%	10%	10%

Table 3: Values of activation energies E_{act} as a function of composition x and temperature.

Activation energies E_{act} (eV)			
x	$\Theta \le 400^\circ C$	$400^\circ C \le \Theta \le 750^\circ C$	
0.0	0.16	1.23	
0.10	0.31	1.16	
0.20	0.18	1.09	
0.30	0.48	1.15	
0.40	0.24	1.19	
	$\Theta \le 200^\circ C$	$200^\circ C \le \Theta \le 500^\circ C$	$500^\circ C \le \Theta \le 750^\circ C$
0.50	0.26	1.28	0.97
0.60	0.36	1.40	1.05
0.70	0.25	1.36	0.95
0.80	0.24	1.34	0.95
0.90	0.24	1.24	
	$\Theta \le 200^\circ C$	$200^\circ C \le \Theta \le 740^\circ C$	
1.00	0.13	1.02	

Appendix

According to authors of [39–43], the Warburg element can be expressed as follows:

$$Z = Z = [R_{\mathrm{Warb}}] \cdot \frac{\mathrm{Tanh}\left[(jA\omega)^n\right]}{(jA\omega)^n}, \tag{A.1}$$

where ω is a pulsation and n is equal to 1/2. In this expression, A is related to the chemical diffusion constant D (in $m^2\cdot s^{-1}$), $A = L^2/D$, L is a length characteristic of reaction process. The term R_W has the dimension of a resistance (in Ω). In the case of heterogeneous interfaces, the n exponent can be different from $n = 1/2$. This model could account for ionic diffusion associated with gas formation at grain boundaries and electrode interfaces: $O^{2-} \leftrightarrow 2e^- + (1/2)O_2$ (g).

Acknowledgments

The authors gratefully acknowledge the Provence-Alpes-Côte d'Azur Regional Council, the General Council of Var, and the agglomeration community of Toulon Provence Mediterranean for their helpful financial supports. This work was developed in the general framework of ARCUS CERES project (2008–2010).

References

[1] L. Bourja, B. Bakiz, A. Benlhachemi et al., "Structural, microstructural and surface properties of a specific CeO_2-Bi_2O_3 multiphase system obtained at 600°C," *Journal of Solid State Chemistry*, vol. 184, no. 3, pp. 608–614, 2011.

[2] J. Kašpar, P. Fornasiero, and M. Graziani, "Use of CeO_2-based oxides in the three-way catalysis," *Catalysis Today*, vol. 50, no. 2, pp. 285–298, 1999.

[3] A. Trovarelli, "Catalytic properties of ceria and CeO_2-containing materials," *Catalysis Reviews*, vol. 38, no. 4, pp. 439–520, 1996.

[4] A. Trovarelli, C. Leitenburg, M. Boaro, and G. Dolcetti, "The utilization of ceria in industrial catalysis," *Catalysis Today*, vol. 50, no. 2, pp. 353–367, 1999.

[5] A. Tschope, W. Liu, M. F. Stephanopoulos, and J. Y. Ying, "Redox activity of nonstoichiometric cerium oxide-based nanocrystalline catalysts," *Journal of Catalysis*, vol. 157, no. 1, pp. 42–50, 1995.

[6] T. Masui, K. Minami, K. Koyabu, and N. Imanaka, "Synthesis and characterization of new promoters based on CeO_2-ZrO_2-Bi_2O_3 for automotive exhaust catalysts," *Catalysis Today*, vol. 117, no. 1–3, pp. 187–192, 2006.

[7] X. Zheng, X. Zhang, Z. Fang, X. Wang, S. Wang, and S. Wu, "Characterization and catalysis studies of CuO/CeO_2 model catalysts," *Catalysis Communications*, vol. 7, no. 9, pp. 701–704, 2006.

[8] O. Demoulin, M. Navez, J.-L. Mugabo, and P. Ruiz, "The oxidizing role of CO_2 at mild temperature on ceria-based

catalysts," *Applied Catalysis B*, vol. 70, no. 1-4, pp. 284–293, 2007.

[9] E. Aneggi, M. Boaro, C. D. Leitenburg, G. Dolcetti, and A. Trovarelli, "Insights into the redox properties of ceria-based oxides and their implications in catalysis," *Journal of Alloys and Compounds*, vol. 408-412, pp. 1096–1102, 2006.

[10] M. Mogensen, N. M. Sammes, and G. A. Tompsett, "Physical, chemical and electrochemical properties of pure and doped ceria," *Solid State Ionics*, vol. 129, no. 1, pp. 63–94, 2000.

[11] R. N. Blumenthal and R. K. Sharma, "Electronic conductivity in nonstoichiometric cerium dioxide," *Journal of Solid State Chemistry*, vol. 13, no. 4, pp. 360–364, 1975.

[12] L. Aneflous, J. A. Musso, S. Villain, J. R. Gavarri, and H. Benyaich, "Effects of temperature and Nd composition on non-linear transport properties in substituted $Ce_{1-x}Nd_xO_{2-\delta}$ cerium dioxides," *Journal of Solid State Chemistry*, vol. 177, no. 3, pp. 856–865, 2004.

[13] P. Shuk, M. Greenblatt, and M. Croft, "Hydrothermal synthesis and properties of $Ce_{1-x}EuxO_{2-\delta}$ solid solutions," *Journal of Alloys and Compounds*, vol. 303-304, pp. 465–471, 2000.

[14] B. Matovic, Z. Dohcevic-Mitrovic, M. Radovic et al., "Synthesis and characterization of ceria based nanometric powders," *Journal of Power Sources*, vol. 193, no. 1, pp. 146–149, 2009.

[15] R. O. Fuentes and R. T. Baker, "Synthesis and properties of Gadolinium-doped ceria solid solutions for IT-SOFC electrolytes," *International Journal of Hydrogen Energy*, vol. 33, no. 13, pp. 3480–3484, 2008.

[16] P. Jasinski, "Electrical properties of nanocrystalline Sm-doped ceria ceramics," *Solid State Ionics*, vol. 177, no. 26–32, pp. 2509–2512, 2006.

[17] P. Shuk, M. Greenblatt, and M. Croft, "Hydrothermal synthesis and properties of mixed conducting $Ce_{1-x}TbxO_{2-\delta}$ solid solutions," *Chemistry of Materials*, vol. 11, no. 2, pp. 473–479, 1999.

[18] L. G. Sillen, *Arkiv for Kemi, Mineralogi Och Geologi*, vol. 12A, 1937.

[19] V. Fruth, A. Ianculescu, D. Berger et al., "Synthesis, structure and properties of doped Bi_2O_3," *Journal of the European Ceramic Society*, vol. 26, no. 14, pp. 3011–3016, 2006.

[20] N. M. Sammes, G. A. Tompsett, H. Näfe, and F. Aldinger, "Bismuth based oxide electrolytes—structure and ionic conductivity," *Journal of the European Ceramic Society*, vol. 19, no. 10, pp. 1801–1826, 1999.

[21] L. E. Depero and L. Sangaletti, "Structural disorder and ionic conduction: the case of Bi_2O_3," *Journal of Solid State Chemistry*, vol. 122, no. 2, pp. 439–443, 1996.

[22] C. N. R. Rao, G. V. S. Rao, and S. Ramdas, "Phase transformations and electrical properties of bismuth sesquioxide," *The Journal of Physical Chemistry*, vol. 73, no. 3, pp. 672–675, 1969.

[23] H. A. Harwig and A. G. Gerards, "Electrical properties of the α, β, γ, and δ phases of bismuth sesquioxide," *Journal of Solid State Chemistry*, vol. 26, no. 3, pp. 265–274, 1978.

[24] P. Shuk, H.-D. Wiemhöfer, U. Guth, W. Göpel, and M. Greenblatt, "Oxide ion conducting solid electrolytes based on Bi_2O_3," *Solid State Ionics*, vol. 89, no. 3-4, pp. 179–196, 1996.

[25] O. Monnereau, L. Tortet, P. L. lewellyn, F. Rouquerol, and G. Vacquier, "Synthesis of Bi_2O_3 by controlled transformation rate thermal analysis: a new route for this oxide?" *Solid State Ionics*, vol. 157, no. 1–4, pp. 163–169, 2003.

[26] F. Schröder and N. Bagdassarov, "Phase transitions and electrical properties of Bi_2O_3 up to 2.5 GPa," *Solid State Communications*, vol. 147, no. 9-10, pp. 374–376, 2008.

[27] F. Schröder, N. Bagdassarov, F. Ritter, and L. Bayarjargal, "Temperature dependence of Bi_2O_3 structural parameters close to the α -δ pphase transition," *Phase Transitions*, vol. 83, no. 5, pp. 311–325, 2010.

[28] S. Hull, S. T. Norberg, M. Tucker, S. Eriksson, C. Mohn, and S. Stølen, "Neutron total scattering study of the δ and β phases of Bi_2O_3," *Dalton Transactions*, no. 40, pp. 8737–8745, 2009.

[29] S. Dikmen, P. Shuk, and M. Greenblatt, "Hydrothermal synthesis and properties of $Ce_{1-x}BixO_{2-\delta}$solid solutions," *Solid State Ionics*, vol. 112, no. 3-4, pp. 299–307, 1998.

[30] X. L. Chen and W. Eysel, "The stabilization of β-Bi_2O_3 by CeO_2," *Journal of Solid State Chemistry*, vol. 127, no. 1, pp. 128–130, 1996.

[31] K. Sardar, H. Y. Playford, R. J. Darton et al., "Nanocrystalline cerium-bismuth oxides: synthesis, structural characterization, and redox properties," *Chemistry of Materials*, vol. 22, no. 22, pp. 6191–6201, 2010.

[32] M. J. Godinho, R. F. Gonçalves, L. P. S Santos, J. A. Varela, E. Longo, and E. R. Leite, "Room temperature co-precipitation of nanocrystalline CeO_2 and $Ce_{0.8}Gd_{0.2}O_{1.9-\delta}$ powder," *Materials Letters*, vol. 61, no. 8-9, pp. 1904–1907, 2007.

[33] J. G. Li, T. Ikegami, Y. Wang, and T. Mori, "Nanocrystalline $Ce_{1-x}Y_xO_{2-x/2}$ ($0 \leq x \leq 0.35$) oxides via carbonate precipitation: synthesis and characterization," *Journal of Solid State Chemistry*, vol. 168, no. 1, pp. 52–59, 2002.

[34] F. Ye, T. Mori, D. R. Ou, J. Zou, and J. Drennan, "Microstructural characterization of terbium-doped ceria," *Materials Research Bulletin*, vol. 42, no. 5, pp. 943–949, 2007.

[35] Y. Ikuma, K. Takao, M. Kamiya, and E. Shimada, "X-ray study of cerium oxide doped with gadolinium oxide fired at low temperatures," *Materials Science and Engineering B*, vol. 99, no. 1–3, pp. 48–51, 2003.

[36] Y. P. Fu and S. H. Chen, "Preparation and characterization of neodymium-doped ceria electrolyte materials for solid oxide fuel cells," *Ceramics International*, vol. 36, no. 2, pp. 483–490, 2010.

[37] D. Johnson, Zview, Impedance software, Version 2.1a, Scribner Associates Inc, (1990–1998).

[38] J. R. Macdonald, "Double layer capacitance and relaxation in electrolytes and solids," *Transactions of the Faraday Society*, vol. 66, pp. 943–958, 1970.

[39] J. R. Macdonald, "Electrical response of materials containing space charge with discharge at the electrodes," *The Journal of Chemical Physics*, vol. 54, no. 5, pp. 2026–2050, 1972, Erratum: electrical response of materials containing space charge with discharge at the electrodes, *The Journal of Chemical Physics*, vol. 56, article, 681, 1972.

[40] J. R. Macdonald, "Impedance spectroscopy: old problems and new developments," *Electrochimica Acta*, vol. 35, no. 10, pp. 1483–1492, 1990.

[41] J. R. Macdonald, "Characterization of the electrical response of high resistivity ionic and dielectric solid materials by immittance spectroscopy," in *Impedance Spectroscopy—Theory, Experiment, and Applications*, E. Barsoukov and J. R. Macdonald, Eds., pp. 264–282, John Wiley & Sons, New Jersey, NJ, USA, 2nd edition, 2005.

[42] C. Ho, I. D. Raistrick, and R. A. Huggins, "Application of AC techniques to the study of lithium diffusion in tungsten trioxide thin film," *Journal of the Electrochemical Society*, vol. 127, no. 2, pp. 343–349, 1980.

[43] B. P. Mandal, S. K. Deshpande, and A. K. Tyagi, "Ionic conductivity enhancement in $Gd_2Zr_2O_7$ pyrochlore by Nd doping," *Journal of Materials Research*, vol. 23, no. 4, pp. 911–916, 2008.